Memo 68
Dynamic range loss due to the retarded baseline effect
M.A.Voronkov, M.H.Wieringa

CSIRO ATNF, Locked Bag 194, Narrabri, NSW 2390, Australia
23 December, 2005

Dynamic range loss due to the retarded baseline effect

M.A. Voronkov, M.H. Wieringa

CSIRO ATNF, Locked Bag 194, Narrabri, NSW 2390, Australia

23 December, 2005

Abstract

In this memo we study the dynamic range loss for wide fields of view caused by unaccounted delay terms due to the retarded baseline effect. It is shown that the effect is quite strong for a 3000 km array (for a field of view as small as 1", the dynamic range is only 3×10^4). Most of this is due to the orbital motion of the Earth and is equivalent to the differential aberration. Although there is no information loss associated with the effect, taking it into account puts an additional stress on the imaging software.

1   Introduction

The Square Kilometre Array (SKA), a proposed next generation synthesis radio telescope, is expected to be a wide-field of view instrument and the same time to provide a high sensitivity, high spatial resolution imaging. This unusual combination of attractive properties puts a significant pressure on the software algorithms to be used for data reduction. Basically, the imaging process can be considered as modelling of the brightness distribution to find the best agreement with the measured visibilities. If this modelling is inaccurate, the residual (unmodelled) emission from the brightest sources will be present in the image as noise because corresponding sidelobes will not be cancelled by the deconvolution algorithm. This limits the ability to study faint sources. In other words, inaccurate modelling limits the dynamic range of the image, which is the

ratio of the flux density of the strongest source in the field to the rms noise in the image produced by the presence of this source. To be a useful instrument the SKA should provide a dynamic range at least 10^6 at 1.4 GHz (Ekers, 2002).

Good examples of the adverse effect of inaccurate modelling occuring in the CLEAN algorithm are the influence of the w-term and the case when the source is located between grid cells studied in detail by Voronkov & Wieringa (2005). Even without the calibration and noise related issues, the true relation between the observed visibilities and the sky brightness (this is called a measurement equation) is not, in general, a 2D Fourier transform, which is a first order approximation only. If, however, the 2D Fourier transform is used in modelling, the dynamic range decreases when the source offset from the phase centre increases. In this memo we present a study of the retarded baseline effect. This is another second order effect, which acts similarly to the w-term introducing an additional phase term in the measurement equation.

2   The retarded baseline effect

The retarded baseline effect is well known and is taken into account in the correlator delay model (e.g. Thompson et al., 1986). The wave front reaches the second antenna at a slightly different time (Fig.1). Therefore, the actual baseline vector corresponding to the spatial frequencies measured by interferometer is the vector between the antenna locations where each antenna receives the wave front. This results in an additional delay term, which is unaccounted for in the static case. This term is, in general, different at different positions on the sky and can be compensated precisely for a single point in the image only, e.g. for the delay-tracking centre, which is usually the same as the phase centre. This compensation takes place at the correlator for phase tracking interferometers. The second complication arises because the coordinate frame of the ground-based array is not an inertial frame. This frame is involved in several rotations with respect to the Solar System barycentric (SSB) reference frame, which can be considered inertial for practical purposes. Therefore, the barycentric velocities of different antennae are different. If they were the same, there would be a constant distortion of the image resulting in a position-dependent shift of the point sources. It reflects the fact that the retarded baseline effect is an another description of aberration (Kaplan 1998). Because this shift is constant in the inertial case, it acts the same way as a true offset. Therefore such a distortion does not affect the dynamic range in the image, although the relative positions of the sources will be wrong. However, because in reality the velocities of different antennae are not the same, the shift will be baseline and time dependent. This can potentially affect the dynamic range.
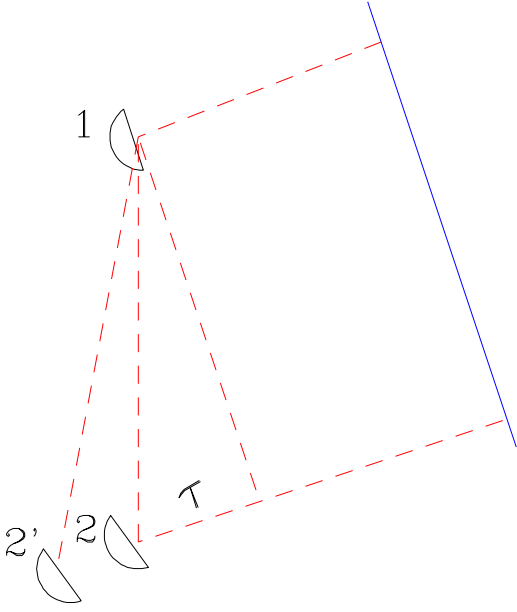
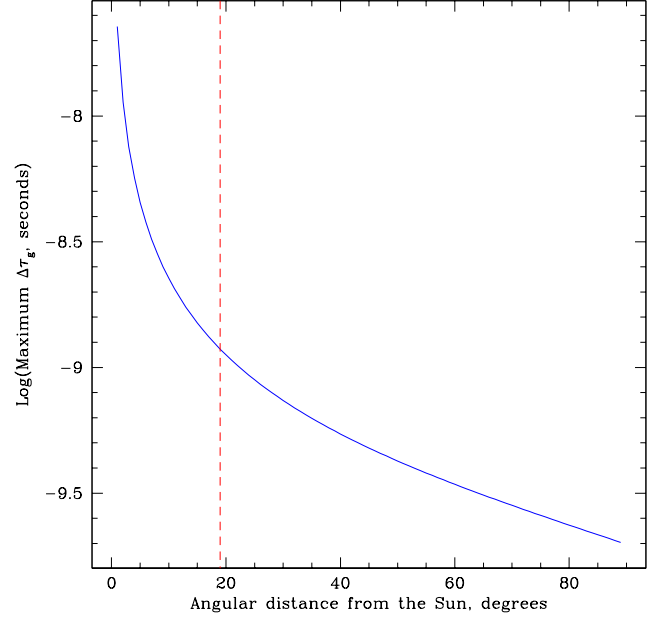Figure 1: Retarded baseline effect: the geometric delay gives the second antenna additional time to move.

Figure 2: The dependence of the maximum possible differential gravitational delay versus the angular distance from the Sun for a 3000 km baseline. The dashed line shows the minimum angular distance where the delay is linear across the 3° field of view.

It is worth to consider the generalized case of the retarded baseline effect using a relativistic delay model developed for astrometry. According to Kaplan (1998), the consensus model for the delay (in a geocentric coordinate time such as TAI) at baseline $\vec{B}$ for an infinitely distant object is

$$\tau = \frac{\Delta\tau_g - \frac{\vec{s}\,\vec{B}}{c}\left[1 - (1+\gamma)U - \frac{1}{c^2}\left(\frac{\dot{E}^2}{2} - \dot{\vec{E}}\,\dot{\vec{r_2}}\right)\right] - \frac{\dot{\vec{E}}\,\vec{B}}{c^2}\left(1 + \frac{\vec{s}\,\dot{\vec{E}}}{2c}\right)}{1 + \frac{\vec{s}\left(\dot{\vec{E}} + \dot{\vec{r_2}}\right)}{c}}, \quad (1)$$

where $\dot{\vec{E}}$ is the velocity of the geocentre with respect to the SSB; $\vec{s}$ is the unit vector of the geometric direction of the studied position; $\dot{\vec{r_2}}$ is the geocentric velocity of the second antenna; U is the total gravitational potential at the geocentre; and γ is a parameterized post-Newtonian (PPN) parameter ($\gamma = 1$ is general relativity). All

3

quantities in the right-hand side of (1) are calculated at the time when the wave front arrives at the first antenna. The term $\Delta\tau_g$ describes the differential gravitational delay (due to slightly different paths in the Solar System of the signal received by different antennae). According to Kaplan (1998) it is calculated for the Sun's field using

$$\Delta\tau_g = (1 + \gamma)\frac{GM_\odot}{c^3}\ln\left(\frac{\vec{s}\,\overrightarrow{R_{1\odot}} + \left|\overrightarrow{R_{1\odot}}\right|}{\vec{s}\,\overrightarrow{R_{2\odot}} + \left|\overrightarrow{R_{2\odot}}\right|}\right), \qquad (2)$$

where $\overrightarrow{R_{1\odot}}$ and $\overrightarrow{R_{2\odot}}$ are the position vectors of the two stations calculated with respect to the Sun. These formulae provide picosecond (ps) accuracy for calculated delays. Assuming that the delay model is precise for the phase centre ($\vec{s_0}$) and the angular dependence is smooth enough to use a linear term only, the residual delay ($\delta\tau$) is determined by the source offset in the image ($\overrightarrow{\delta s}$) and the delay gradient

$$\delta\tau = \tau - \tau_0 \approx \left.\frac{\partial\tau}{\partial\overrightarrow{\delta s}}\right|_{\vec{s}=\vec{s_0}}\overrightarrow{\delta s}, \qquad (3)$$

where τ_0 is the geometric delay for the phase centre. Note that due to a logarithmic dependence of the gravitational delay given by (2), the linear approximation implied by (3) is not valid close to the Sun. To be able to linearize (2), the Sun avoidance angle is $\varphi \gg \cos^{-1}(1 - FOV_{rad})$, where FOV_{rad} is the field of view in radians. For a 3° field of view this yields the Sun avoidance angle more than 19°. Because low frequency observations (e.g. HI) are unlikely to be carried out close to the Sun due to solar interference, a linear approximation of (2) seems to be reasonable. Therefore, the residual gravitational delay is

$$\delta\tau_g \approx \frac{\partial\Delta\tau_g}{\partial\overrightarrow{\delta s}}\overrightarrow{\delta s} \approx -(1 + \gamma)\frac{GM_\odot}{c^3}\frac{\vec{B}\,\overrightarrow{\delta s}}{\vec{s_0}\,\overrightarrow{R_\odot} + \left|\overrightarrow{R_\odot}\right|}\left(1 - \frac{\vec{s_0}\left(\dot{\vec{E}} + \dot{\vec{r_2}}\right)}{c}\right), \qquad (4)$$

where $\overrightarrow{R_\odot}$ is the Earth's position with respect to the Sun. The smallest angular distance from the Sun allowed by this linear approach corresponds the maximum possible residual delay due to the Sun's gravity. Assuming a 3000 km baseline and a 3° field of view (i.e. $\varphi > 19^o$), one get an estimate $|\delta\tau_g| \leq 100$ ps (a 200 ps delay across a 3° field of view, see Fig. 2).

4

The maximum possible values for other terms in the derivative of (1) assuming a 3000 km baseline and a 3° field of view can be estimated in a similar way taking into account that $\left|\dot{\vec{E}}\right| \approx 30$ km s^{-1} and $\left|\dot{\vec{r_2}}\right| < 0.5$ km s^{-1}

$$\left|\frac{\dot{\vec{B}}\,\vec{\delta s}}{c}\right| \leq 3 \times 10^{-4}\text{ s}, \qquad \frac{|\dot{\vec{B}}|}{c} \leq 0.01\text{ s},$$

$$\left|\frac{\dot{\vec{E}}}{c}\right| \leq 10^{-4}, \qquad \left|\frac{\dot{\vec{r_2}}}{c}\right| \leq 2 \times 10^{-6}, \tag{5}$$

$$\left|\frac{\dot{\vec{E}}\,\dot{\vec{r_2}}}{c^2}\right| \leq 2 \times 10^{-10}, \qquad \left|\frac{\dot{\vec{E}}\,\vec{\delta s}}{c}\right| \leq 3 \times 10^{-6}.$$

Taking these estimates and $(1+\gamma)U = 19.7 \times 10^{-9}$ (Kaplan 1998) into account and retaining only terms which exceed 0.1 ps, (3) is equivalent to

$$\delta\tau = \delta\tau_g - \frac{\dot{\vec{B}}\,\vec{\delta s}}{c}\left(1 - \xi + \eta\right) + \zeta, \tag{6}$$

where

$$\xi = (1+\gamma)\,U + \frac{|\dot{\vec{E}}|^2}{2c^2} \sim 2.5 \times 10^{-8} \tag{7}$$

is a constant stretch of the image related to the time retardation, which does not affect the dynamic range, while η and ζ are baseline-dependent terms

$$\eta = \frac{\dot{\vec{E}}\,\dot{\vec{r_2}}}{c^2} + \left(\frac{\left(\dot{\vec{E}} + \dot{\vec{r_2}}\right)\vec{s_0}}{c}\right)^2 - \frac{\left(\dot{\vec{E}} + \dot{\vec{r_2}}\right)\vec{s_0}}{c}, \tag{8}$$

$$\zeta = \frac{(\dot{\vec{E}}\,\dot{\vec{B}})(\dot{\vec{E}}\,\vec{\delta s})}{2c^3} + \frac{(\vec{s_0}\dot{\vec{B}})\left(\left(\dot{\vec{E}} + \dot{\vec{r_2}}\right)\vec{\delta s}\right)}{c^2}\left(1 - \frac{2(\dot{\vec{E}} + \dot{\vec{r_2}})\vec{s_0}}{c}\right). \tag{9}$$

Recall that the delay model (1) has picosecond accuracy. Deriving (7)-(9) we have assumed that no effects unmodelled by (1) give an extra delay which exeeds 0.1 ps in the 3° field of view. For snap-shot observations with a sufficiently compact array (i.e. if the term $\left(\dot{\vec{E}} + \dot{\vec{r_2}}\right)$ can be assumed constant), the presence of η does not affect the

dynamic range. It is equivalent to a stretch of the image (the last term in (8) is the largest by absolute value, so $|\eta| \leq 10^{-4}$), which is, in general, time-dependent. The nature of this stretch is mainly a difference of aberration across the field of view. The effect is minimal when the direction to the phase centre is orthogonal to the velocity vector of antennae. For large arrays, the velocities of antennae are significantly different due to diurnal rotation. Therefore, in this case the term η becomes baseline-dependent. The term ζ contains baseline-dependent terms, which cause a distortion more complex than a simple stretch of the image and can affect the dynamic range. These terms are less than 30000 ps and, in general, vary in time.

3 Simulations

All simulations have been done in the AIPS++[1] environment in a similar way to Voronkov & Wieringa (2005). First, the visibilities corresponding to a point source at a given offset from the phase (and delay-tracking) centre were simulated. This dataset was then processed using the Cotton-Schwab clean algorithm (with optimization and uniform weights; see Voronkov & Wieringa, 2005) and the dynamic range was determined as a ratio of the known flux of the point source to the rms in the residual image. However, in these simulations the equation (6) has been used to calculate the delays instead of

$$\delta\tau_0 = -\frac{\vec{B}\,\vec{\delta s}}{c}, \tag{10}$$

introducing an additional phase term to the equation for visibilities. In order to investigate individual effects contributing to the dynamic range loss some models have taken into account just the gravitational delay (ξ, η and ζ are set to 0), the delay due to Earth orbital motion ($\delta\tau_g$ and $\vec{r_2}$ are set to 0), or just the delay due to diurnal rotation ($\delta\tau_g$ and $\vec{E}$ are set to 0). In all simulations the phase centre has been fixed at -50° of declination and was in transit at the array core at the middle of the simulated observations if not stated otherwise.

The simulated array layout (Fig.3) was different from that used by Voronkov & Wieringa (2005). It contained 114 antennae with the largest baseline of approximately 2600 km and was one of the reference layouts given as an example to SKA site proposers. It is probably a more realistic layout for the SKA than the unconstrained spiral

---

[1]The AIPS++ software package, http://aips2.nrao.edu, is developed by the National Radio Astronomy Observatory (NRAO), which is a facility of the National Science Foundation operated under cooperative agreement by Associated Universities, Inc.
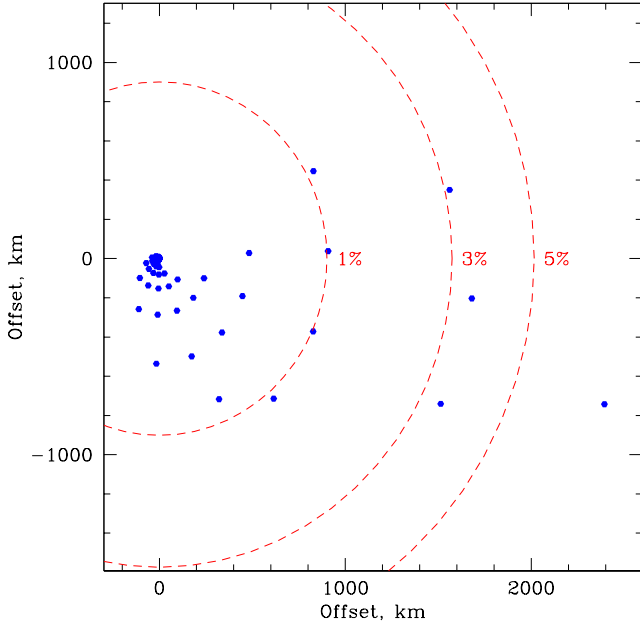
Figure 3: The array layout used for simulations in the orthographic projection (as seen from the phase centre transiting at the core site). The core is located at $-26^o 21'$. The dashed circles show the depth below the tangential plane passing through the array core. Numbers are given as a fraction from the Earth radius.
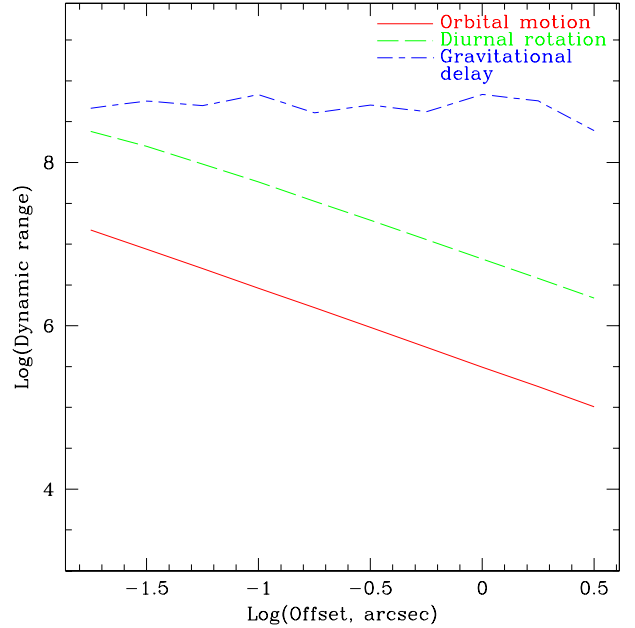
Figure 4: Dynamic range loss due to various effects in the delay model. Snapshot observations on 21st of September are simulated.

used by Voronkov & Wieringa (2005), which had 300 antennae with a largest baseline of approximately 6300 km.

4   Results

The dependence of dynamic range versus source offset for various delay models are shown in Fig. 4. The orbital motion of the Earth limits the dynamic range at much lower values than the other effects. Even when the offset is as small as 300 milliarcseconds, the dynamic range is below the SKA requirement of 10^6. This limitation is even a bit stronger than that in the case of an unaccounted w-term (see Voronkov & Wieringa, 2005). The diurnal rotation of the Earth as well as the gravitational term put a weaker constraint on the dynamic range (Fig. 4). For these effects the dynamic range is above 10^6 for source offsets less than 5". The curve corresponding to the diurnal rotation
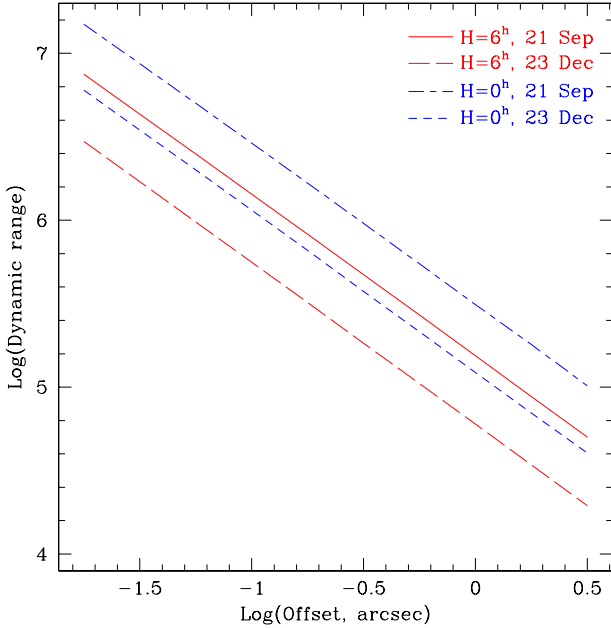
Figure 5: Dynamic range loss due to the orbital motion of the Earth. Snap-shot observations at two different dates are simulated. The phase centre has two different hour angles at the array core: $H=0^h$ (transit) and $H=6^h$.
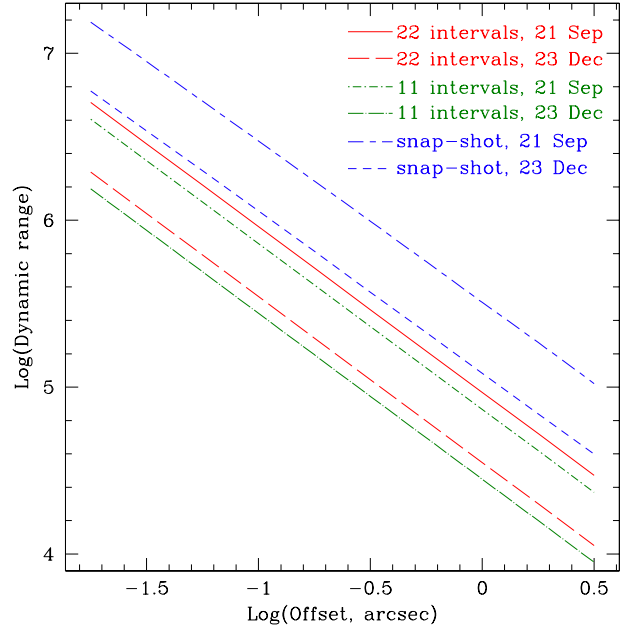
Figure 6: Dynamic range loss in the case of snap-shot and prolonged observations (11 snap-shots executed hourly and 21 snap-shots executed every 30 minutes). All effects considered in section 2 are included.

shows a steady decrease of the dynamic range with source offset. Therefore, for a wide field of view, this effect should also be taken into account.

Fig. 5 shows the dynamic range loss due to the retarded baseline effect caused by the Earth's orbital motion. As mentioned above, the effect can be considered as differential aberration. Therefore, it is expected to be the largest when the vector of the orbital velocity points to the phase centre. A set of curves in Fig. 5 represents various orientations of the orbital velocity vector with respect to the phase centre direction due to different dates and times (given as the hour angle of the phase centre at the array core) of observations. The resulting dynamic range varies by almost an order of magnitude. The situation does not change much for long observations (Fig. 6). To model long observations we simulated two datasets containing 11 or 21 snap-shots distributed uniformly over a range of hour angles from $H=-5^h$ to $H=5^h$, one snap-shot per hour and per 30 minutes, respectively. All effects described in section 2 (gravitational delay, orbital motion, diurnal rotation) have been included in the simulations, although the orbital motion contributes the most to the dynamic range loss. Long observations give a lower dynamic range throughout the whole range of simulated offsets in com-

8

parison to snap-shot observations carried out at the same date. However, the difference between 11 and 22 snap-shots is small. This indicates the dynamic range loss is due to systematic changes in the delays throughout the simulated observations (due to the Earth's orbital motion). Fig. 5 shows that the dynamic range varies a lot with hour angle for snap-shot observations as the orientation of the orbital velocity vector with respect to the phase centre direction changes. Considered as aberration, the effect is equivalent to the position and time dependent shift of the source in the image domain. The time dependence is systematic rather than random and, hence, causes a decrease of the dynamic range in Fig. 6.

There is no information loss associated with the retarded baseline effect. The formulae from section 2 allow removal of the residual delay for any given point in the image. Effectively, this shifts the delay-tracking centre to a new position. The situation is somewhat equivalent to the w-term problem (non-coplanar baselines). Therefore, an algorithm, where the whole field of view is split into a number of small facets, is possible. Each facet should be small enough to neglect the retarded baseline effect. However, to achieve a dynamic range of 10^6 the size of each facet should be of the order of ten milliarcseconds. This is close to the grid cell size determined by the largest baseline (about 5 milliarcseconds at 1.4 GHz for a 3000 km baseline). Therefore, an algorithm decomposing the sky into a number of discrete components, which can be accurately modelled (e.g. the Cotton-Schwab CLEAN algorithm), may be a better choice. Correcting for the retarded baseline effect puts an additional burden on the software. Although the Cotton-Schwab CLEAN algorithm can account for this effect along with the w-term with no further performance penalty, it is very expensive computationally due to the visibility-based cycle. More efficient approaches should be developed to tackle the problem. The similarity between the w-term and the retarded baseline effect suggests that a modification of the w-projection algorithm (Cornwell et al., 2003) could be developed. However, the retarded baseline effect is more complex and depends on a larger number of time variable parameters (e.g. antenna velocities, orientation with respect to the Sun). Therefore, further investigations are required to assess the feasibility of such an approach and its performance.

5   Conclusions

1. The retarded baseline effect must be taken into account in wide-field of view experiments which require high resolution and high dynamic range imaging.

2. The largest loss of dynamic range is due to the orbital motion of the Earth. The

9

effect is equivalent to differential aberration (accross the field of view) and is quite strong (stronger than the w-term effect), limiting the dynamic range at the level of 3×10^4 for a 1" field of view for observations with a 3000 km array at 1.4 GHz.

3. Other effects on the dynamic range we considered (diurnal rotation of the Earth, differential gravitational delay) are a few orders of magnitude weaker than the effects of the orbital motion.

4. The retarded baseline effect does not cause loss of information and can be corrected in software. This correction is straightforward in the component based Cotton-Schwab approach, but is computationally very expensive due to the visibility based cycle.

References

Cornwell T.J., Golap K., Bhatnagar S., 2003, EVLA Memo 67

Ekers R., Technical Specification for the SKA. SKA Memo, 4, 2002

Kaplan G.H., High-precision algorithms for astrometry: a comparison of two approaches, 1998, AJ, 115, 361

Thompson A.R., Moran J.M., Swenson G.W. Jr., Interferometry and Synthesis in Radio Astronomy, John Wiley & Sons, New York, 1986

Voronkov M.A., Wieringa M.H., The Cotton-Schwab CLEAN at ultra-high dynamic range, Experimental Astronomy, 2005, in press